processes

MDPI

*Article*

# Experimental Investigation of the Relationship of Failure Mode and Energy Dissipation in Grouted Rockbolt Systems under Pullout Load

**Shuisheng Yu *, Yawei Wang, Honghao Yang and Shucan Lu**

School of Architectural Engineering, Zhongyuan University of Technology, Zhengzhou 450007, China; 2021109335@zut.edu.cn (Y.W.); 2021109358@zut.edu.cn (H.Y.)
* Correspondence: yuss.1987@zut.edu.cn

**Abstract:** In underground engineering, the deformation of surrounding rock caused by "three heights and one disturbance" leads to the failure of grouted rockbolt systems, which causes huge economic losses to the mining industry. The research shows that the failure process of grouted rockbolt systems is the result of energy accumulation and release, but the relationship between failure mode and energy dissipation is rarely studied. Based on this, the load transfer behavior, energy dissipation, failure mode and failure mechanism of the grouted rockbolt systems are investigated from the perspective of energy in this study using the indoor pullout test. Test results show that the load decreases rapidly, and the absorbed energy decreases due to the whole-body splitting crack. The absorbed energy of the specimen in the splitting crack mode is lower than that in the pullout failure mode. When the pullout load reaches its peak, the pullout load of the specimen with split failure mode decreases sharply. Meanwhile, the load of the specimen with pullout failure mode is relatively slow, and the energy absorption rate decreases gradually due to the occurrence of cracks. However, the reduction in the energy absorption rate under pullout failure is lower than that under split failure. The radial pressure in the grouted rockbolt systems increases due to the wedge action. When the radial pressure exceeds the tensile strength of concrete, the specimen will experience split failure, otherwise pullout failure will occur.

**Keywords:** pullout load; grouted rockbolt systems; failure mode; energy dissipation; load transfer



**Citation:** Yu, S.; Wang, Y.; Yang, H.; Lu, S. Experimental Investigation of the Relationship of Failure Mode and Energy Dissipation in Grouted Rockbolt Systems under Pullout Load. *Processes* **2023**, *11*, 2601. https://doi.org/10.3390/pr11092601

Academic Editors: Yang Li, Guanglei Zhou and Feiyue Liu

Received: 1 August 2023
Revised: 27 August 2023
Accepted: 29 August 2023
Published: 31 August 2023



## 1. Introduction

The process of deep mining is prone to the occurrence of complex geological conditions, such as "three heights and one disturbance" (high ground stress, high seepage pressure, high earth temperature and mining disturbance) and extremely soft rock. These severely influence the failure forms of surrounding rock, such as rock burst, instantaneous large deformations of rock burst, and slow large deformations of soft rock [1–5]. The traditional rockbolt support system is the most commonly used support method in mining, and has achieved good economic and social benefits. However, with the continuous increase in mining depth and intensity, the physical and mechanical properties of surrounding rock become more complicated [6,7]. When traditional rockbolt is faced with instantaneous large deformation or slow large deformation damage, it often causes rockbolt breakage, surrounding rock collapse, and other hazards, which leads to the failure of the rockbolt anchorage structure [8–11]. The deformation process of surrounding rock is accompanied by the accumulation and release of energy [12–14]. To solve these problems, researchers worldwide developed a variety of energy-absorbing rockbolts from the perspective of the energy absorption of grouted rockbolt systems. However, energy-absorbing rockbolts cannot be widely used in mining due to limitations such as high cost, complex structure, and unstable energy release [15–17]. Therefore, the analysis of the energy absorption of

traditional grouted rockbolt systems holds great significance for the design of rockbolt support system in deep mining.

According to the research, the failure of the grouted rockbolt systems is because the anchorage interface between the rockbolt and the anchoring agent is a thin layer of cement mortar; when the load on the rockbolt gradually increases from zero, the bonding stress between the anchorage interface also increases gradually, and when the bonding stress is greater than the shear strength of the concrete layer, the concrete layer breaks and the anchorage interface becomes unglued [18,19]. The bearing capacity of the grouted rockbolt systems decreases, which leads to the deformation of surrounding rock and eventually leads to the failure of the grouted rockbolt systems. Therefore, in order to deeply understand the bonding stress distribution at the anchorage interface, researchers have done a lot of experimental research on the load transfer mechanism of grouted rockbolt systems. According to the pullout test, in the process of load transfer, the axial force and shear stress at the loading end are the largest, and there is a negative exponential distribution in the anchorage zone. Under the action of transverse tension, the sliding displacement corresponding to the peak bond strength first increases with the increase in the transverse tension, and then remains unchanged or decreases with the increase in the transverse tension. However, under different lateral pressures, the rockbolt will have a delayed bonding response. The peak bond strength and friction resistance are delayed to different degrees, and the delayed debonding will significantly affect the service life of the rockbolt [20–22]. Other scholars believe that the failure of the grouted rockbolt systems depends on the strength of cement mortar, and the split failure mode is caused by the wedge-shaped action of the rockbolt ribs [23,24]. In addition, in the process of in situ pullout, when the anchorage length increases from 2 m to 4 m, the slip amount can be reduced by 20%, and the anchorage strength and displacement of the rockbolt will also decrease with the increase in the horizontal installation angle [25,26]. Although good results have been achieved in the load transfer behavior of rockbolt, the influence of energy on grouted rockbolt systems is ignored, and its failure process is the result of energy accumulation and release. Yu et al. [23] studied energy dissipation in the process of rockbolt pullout. The results show that the energy absorbed by the rockbolt increases with the strength of cement mortar when the diameter of the rockbolt is the same. However, the relationship between the failure mode and energy dissipation of grouted rockbolt systems is not analyzed.

To address this problem, this study carries out a pullout test on the grouted rockbolt systems and analyzes the load transfer mechanism of the rockbolt under different failure modes from the perspective of energy. The relationships between the energy dissipation and failure modes are verified, and the failure mechanism of the grouted rockbolt systems is analyzed, which provides a reference for the design of different rockbolt support systems in the deep mining process.

## 2. Test Design

### 2.1. Specimen Design

C30 concrete is used in this study to simulate the surrounding rock, whose use is mainly due to the large size of the sample, which is inconvenient and ineffective for rock samples. The concrete sample constitutes a hollow cylinder with an inner and outer diameter of 40 and 150 mm, respectively, and a length of 500 mm; the dimension parameters of the grouted rockbolt systems are shown in Figure 1. The raw materials are: (1) ordinary Portland cement with a 28-day compressive strength of 42.5 MPa produced in the Fengshou Cement Plant of Xinxiang City; (2) natural river sand with a grain diameter of 0.3–2.36 mm used as fine aggregate; (3) gravel with a grain diameter of 5–20 mm used as coarse aggregate; (4) tap water. The mixing ratio of the concrete sample is cement:water:fine aggregate:coarse aggregate = 1:0.47:1.3:3.02. Cement mortar is used as the anchoring agent, and its raw materials include: (1) ordinary Portland cement with 28-day compressive strength of 42.5 MPa produced at the Fengshou Cement Plant of Xinxiang City; (2) natural river sand

with a grain diameter of 0.3–1.16 mm used as fine aggregate; (3) tap water. To ensure that the rockbolt slips and cement mortar can be easily injected into the rockbolt hole without being pulled off, the mixture ratio of cement mortar is set at 0.47:1:1.3. The matching of cement mortar and concrete is shown in Table 1.

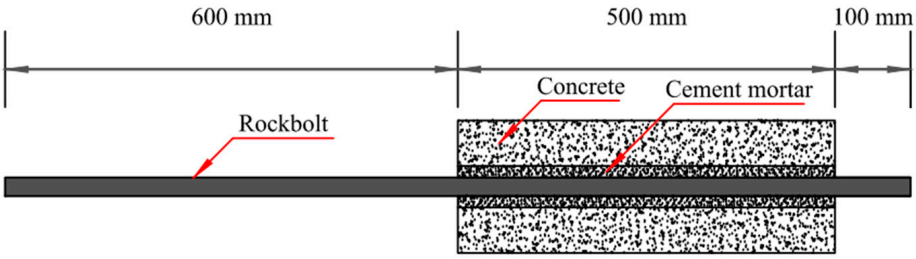


**Figure 1.** Schematic diagram of grouted rockbolt systems.

**Table 1.** Mixing proportions of concrete and cement mortar.

| Raw Material | Water | Cement | Sand | Stone |
|---|---|---|---|---|
| Concrete | 0.47 | 1 | 1.3 | 3.02 |
| Cement mortar | 0.47 | 1 | 1.3 | 0 |

The rockbolt is made of a HRB400 seismic threaded steel bar with a 25 mm diameter, produced by Qinyang Hongda Iron and Steel Co., Ltd. (Jiaozuo China), with a yield strength of 400 MPa, ultimate strength of 540 MPa, and length of 1200 mm, of which 500 mm is anchored in concrete. To simulate the field test, a detachable split cylindrical mold was developed to produce the rockbolt anchorage structure sample. Firstly, a round steel bar with a diameter of 40 mm is placed in the center of the mold, and at the same time, concrete is poured into the mold on a vibrating table and vibrated to ensure the discharge of bubbles. After the concrete samples are cured for two days, the upper and lower gaskets are removed, the round steel rod is pulled out, and the rockbolt is fixed in the center of the round hole; the cement mortar mixed in proportion is poured in, and the iron wire is used to stir at the same time. Finally, the sample is cured in the laboratory for 28 days and then tested. The manufacturing process of the sample is shown in Figure 2.

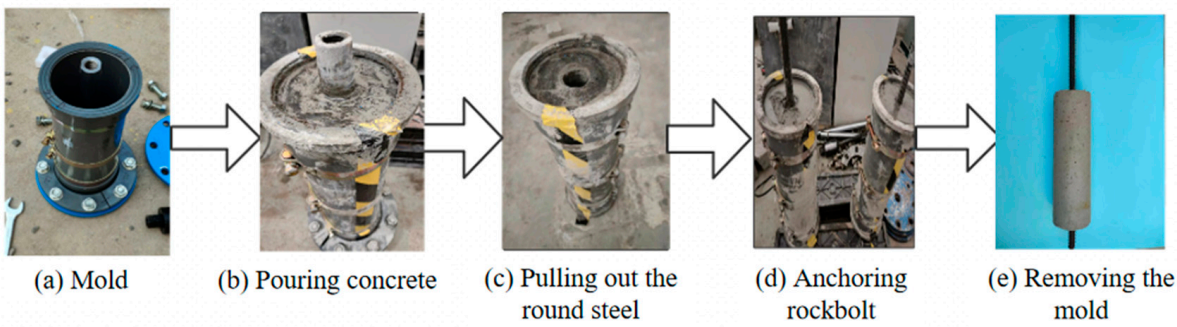


**Figure 2.** Manufacturing process of grouted rockbolt system sample for field test simulation.

### *2.2. Test Procedure*

The device used in the test comprises the rockbolt loading system, the force detection test system, and the displacement detection test system. The schematic diagram for the pullout test is shown in Figure 3, which shows that the device can apply load and detect the change in force and displacement in the process of the rockbolt pullout.

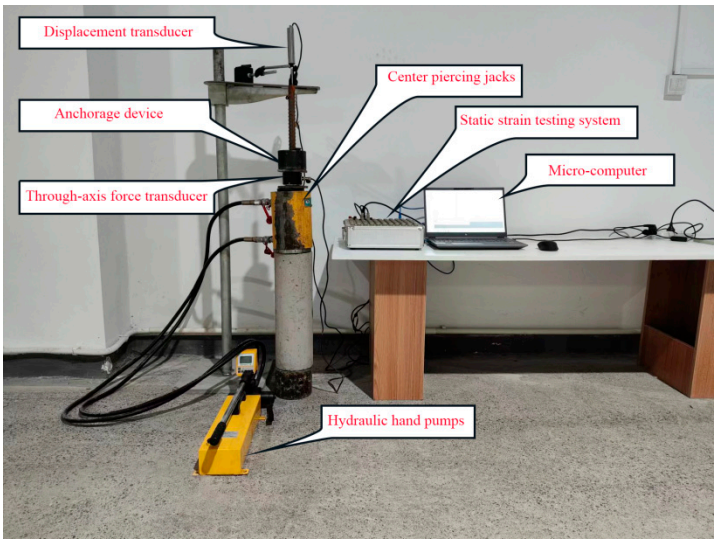


**Figure 3.** Schematic diagram of pullout test.

The rockbolt loading system employs the ZY-50T rockbolt pulling instrument produced by Shijiazhuang Zhuo Pu Science and Technology Co., Ltd. (Shijiazhuang, China), with a measuring range of 0–500 kN, which mainly includes hydraulic hand pumps and center piercing jacks. A hydraulic hand pump was utilized to apply monotonic loads to the penetration jacks followed by pullout loads to the grouted rockbolt systems specimens.

The force detection test system employs the through-axis force transducer produced by Bengbu Sensor System Engineering Co., Ltd. (Bengbu, China), whereas the displacement detection test system uses the YWC-50 displacement transducer produced by Liyang Chaoyuan Instrument Factory.

In the test, first, the hydraulic hand pump is operated at a slow and uniform speed to apply the pulling load to the rockbolt. The shaft-through force transducer measures the pulling load and connects with the DH-3816N static strain testing system produced by Jiangsu Donghua Testing Technology Co., Ltd. (Taizhou China) to record it. The displacement transducer is used to record the moving displacement of the rockbolt at the loading end with respect to the concrete specimen, and stops the loading when the rockbolt slips completely. The pulling load and displacement are all stored in the micro-computer through the static strain testing system.

## 3. Energy Characteristics during Pullout Process

In the process of deep mine mining, the stress state equilibrium of the original rock is lost due to the unloading of the rock excavation, leading to a redistribution of the rock stress and the energy transfer and accumulation in the rockbolt support system acting on the rock. In fact, the rockbolt shows a pulling action, which is the process of energy absorption in the rockbolt, so the degree of the pulling process of energy absorption can reflect whether the mechanical properties of the rockbolt are good or bad. The first law of thermodynamics states that all the work done by the external force during the bond destruction process is causes the change in internal energy at the interface, as in, all mechanical energy is converted into the change of internal energy at the interface, as is represented by Equation (1) [27]. However, the increase in $U_e$, $U_p$ and $U_s$ can increase the interfacial energy, while the increase in $U_m$ will decrease the interfacial energy. Therefore, the conservation of energy in the process of deformation and failure of the interface reveals the transformation and balance between the mechanical energy $W$ generated by external work and the change of internal energy $\Delta U$ in the interface, which can be expressed by Equation (2) [27].

$$\Delta U = f(U_e, U_p, U_s, U_m) \quad (1)$$

where $U_e$ is the elastic deformation energy, $U_p$ is the plastic deformation energy, $U_s$ is the surface energy and $U_m$ is the radiant energy.

$$W = \Delta U \tag{2}$$

Cement mortar likewise absorbs energy during rockbolt pullout; however, the strain energy absorbed in the cement mortar is difficult to measure in the test, and its proportion is very small, such that the work done by the pullout load P stored in the cement mortar as strain energy is negligible. The energy loss during loading is omitted, such that the change of energy in the anchorage interface is numerically equal to the strain energy in the rockbolt, and the strain energy in the rockbolt is numerically equal to the work done by the external force, as shown in Equation (3) [23,28,29]; the energy absorbed by the rockbolt during pulling is $W$, expressed as:

$$W = V \times \int_0^{\varepsilon} \sigma d\varepsilon = \int_0^{s} P ds \tag{3}$$

where $V$ is the volume of the rockbolt at the loading end, σ is the axial stress of the rockbolt at the loading end, $\varepsilon$ is the strain of the rockbolt at the loading end and $S$ is the displacement of the rockbolt at the loading end.

As an example, a 25 mm-diameter rockbolt rod was used to conduct pullout tests on the bond rockbolt age structure to obtain the rockbolt load–displacement relationship, the peak load value load of the rockbolt, and the corresponding displacement of the peak load, as shown in Figure 3. According to Equation (1), the total energy absorbed by the rockbolt in the pulling process displacement ranged 0–12 mm, whereas the energy absorbed by the rockbolt in the elastic phase, softening phase, and residual phase, respectively, for Specimens #1–8 is shown in Table 2.

**Table 2.** Energy absorption of different rockbolts during pullout process.

| Specimen Number | Peak Load (kN) | Peak Load Displacement (mm) | Energy Absorption in Elastic Phase (J) | Energy Absorption in Softening Phase (J) | Energy Absorption in Residual Phase (J) | 0–12 mm Total Energy Absorption (J) | Failure Mode |
|---|---|---|---|---|---|---|---|
| 1# | 120 | 1.28 | 72.26 | 117.89 | 25.95 | 216.10 | split |
| 2# | 144.14 | 1.0 | 100.44 | 211.52 | 53.24 | 365.20 | split |
| 3# | 149.29 | 1.24 | 108.46 | 151.52 | 36.24 | 296.22 | split |
| 4# | 188.29 | 1.14 | 151.38 | 207.9 | 61.12 | 420.40 | split |
| 5# | 103 | 1.8 | 129.17 | 277.72 | 127.71 | 534.60 | pullout |
| 6# | 126.29 | 1.23 | 105.96 | 298.81 | 130.02 | 534.79 | pullout |
| 7# | 166.29 | 1.32 | 187.96 | 398.22 | 142.47 | 728.65 | pullout |
| 8# | 192 | 1.5 | 161.17 | 438.93 | 150.1 | 750.20 | pullout |

## 4. Test Results and Analysis

### *4.1. Relationship between Energy Dissipation and Load Transfer in Grouted Rockbolt Systems during the Pullout Process*

The relationship between the rockbolt pullout load and displacement during the pullout process is shown in Figure 4. In the early stage of loading, the load–displacement relationship tends to a straight line, the displacement is small, and the load grows fast, which is because the bond stress caused by the load acting on the rockbolt is mainly provided by the chemical adhesive force between the rockbolt and the anchoring agent, and the chemical adhesive force between the anchorage interface is small. As a result, the constraints that the rockbolt needs to overcome in the pullout process are small, so the energy absorbed by the rockbolt is relatively small in the initial loading stage, as shown in

Figure 5. With the increase in load, the load–displacement relationship deviates from the straight line, and the anchorage interface between the rockbolt and the anchoring agent is a thin layer of cement mortar. When the surfaces of the rockbolt and cement mortar fall off, the chemical adhesive force gradually disappears, the friction resistance of the anchorage interface is gradually mobilized, and the bonding stress is provided by the mechanical bite force and friction force. The bonding stress gradually increases, and the loading end begins to slip under the action of the bonding stress, while the energy absorbed rate increases linearly before reaching the peak load. When the bond stress is greater than the shear strength of the cement mortar, cracks parallel to the rockbolt are first formed at the loading end of the cement mortar layer, and gradually develop to the free end, and the energy absorbed by the rockbolt increases sharply. The crack expands under the action of bonding stress. Then, the load decreases sharply, and the energy absorption rate gradually slows down with the decrease in the load. The anchorage interface is first unglued at the loading end and develops toward the free end, which leads to the breaking and accumulation of anchoring agent and forces the radial pressure inside the concrete. When the radial pressure on the concrete is greater than its circumferential tensile strength, cracks parallel to the rockbolt will develop on the concrete ends. The anchorage interface at the loading end produces cracks parallel to the rockbolt, which continuously develop in the direction that makes the rockbolt unglued during the pullout process. The failure mode is similar to type II of fracture mechanics, until the interface is completely unglued [30]. At this time, the amount of slip of the bolt increases and the bonding stress decreases. As can be seen from Table 2, the maximum energy absorption in the softening stage during the entire pullout process is 117.89 J, 211.52 J, 151.52 J, 207.9 J, 277.72 J, 298.81 J, 398.22 J and 438.93 J, respectively, which all represent more than 50% of the total energy absorption. As can be seen from Figures 4 and 5, when the anchorage interface is completely unglued, the pullout load gradually decreases in repeated fluctuations, the energy absorption rate continues to slow down, and the anchorage interface enters the residual stress stage.

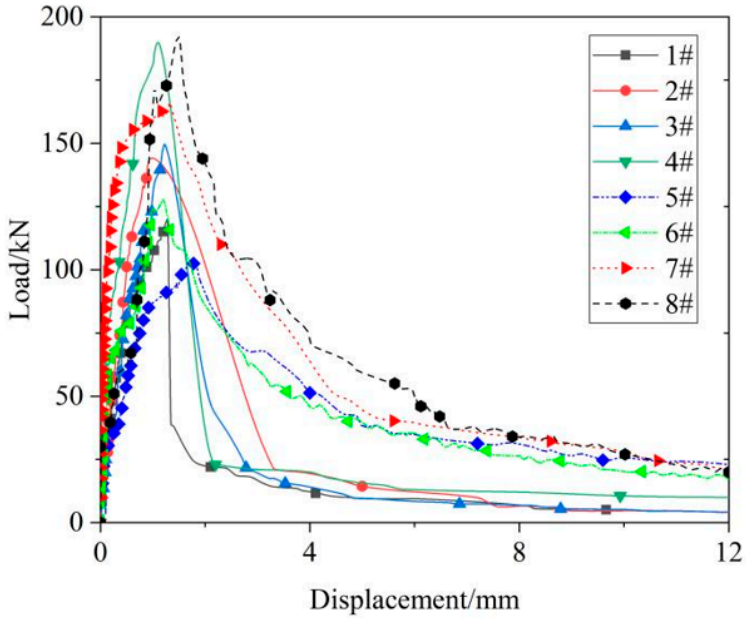


**Figure 4.** Pullout load–displacement relationship.

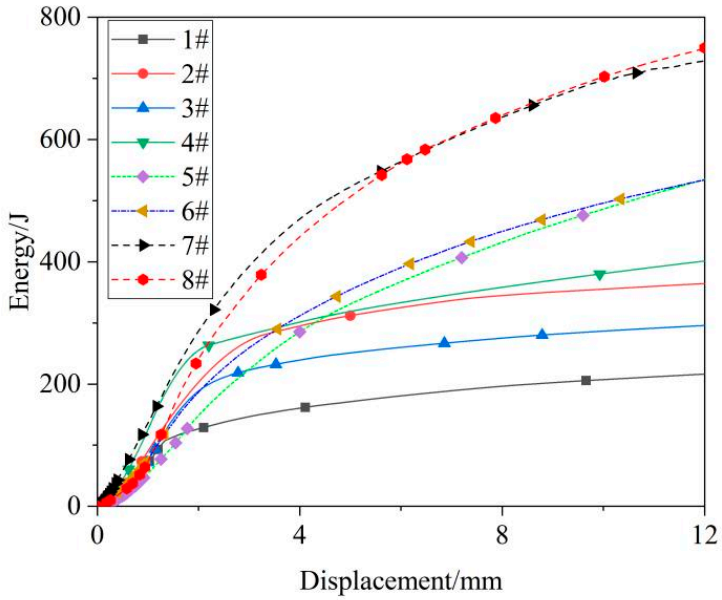


**Figure 5.** Energy–displacement relationship.

*4.2. Relationship between Energy Dissipation and Failure Mode of Grouted Rockbolt Systems*

In the process of pulling out, the function of the load acting on the rockbolt causes a change in the internal energy at the anchorage interface, that is, the mechanical energy is converted into internal energy. Ignoring the energy lost during the loading process, the energy absorbed by the rockbolt is numerically equal to the change in the energy at the anchorage interface. Table 2 indicates that the failure mode of specimens #2 and 4 is split failure, whereas the failure mode of specimens #6 and #8 is failure. When the total pullout displacement is 12 mm, the energy absorption of specimens undergoing pullout failure is higher than that of the specimens undergoing split failure. As shown in Figure 6, for specimens #2 and 4, when split failure occurs in the specimen, it is accompanied by the occurrence of a crisp ringing sound, and the surface of the specimen produces a through splitting crack. Figure 7 shows the load to energy displacement relationship for specimens #2 and 4. The energy absorption rate of specimen #4 is higher than that of specimen #2 until the end of the softening phase, and the total energy absorbed by specimen #4 in the elasticity and softening phases is 359.28 J higher than that absorbed by specimen #2—311.96 J. The softened interface develops from the loaded end to the free end, the unsoftened interface gradually decreases, and the crack development rate is higher than the load reduction rate, resulting in the increase in bonding stress at the unsoftened interface. Therefore, the anchoring agent is first shear damaged at the free end and gradually extended to the free end. In the softening stage, the load and load reduction rate of specimen #4 are higher than those of specimen #2, which leads to the complete fracture of the anchoring agent of specimen #4, and a small amount of the anchoring agent is pulled out with the rockbolt at the free end of specimen #2 (Figure 6). The broken anchoring agent will further increase the mechanical bite force of the anchorage interface, so the bonding stress of specimen #4 is greater than that of specimen #2 during the pullout process. As a result, the energy absorption rate of specimen #2 tends towards 0, which is significantly lower than that of specimen #4.

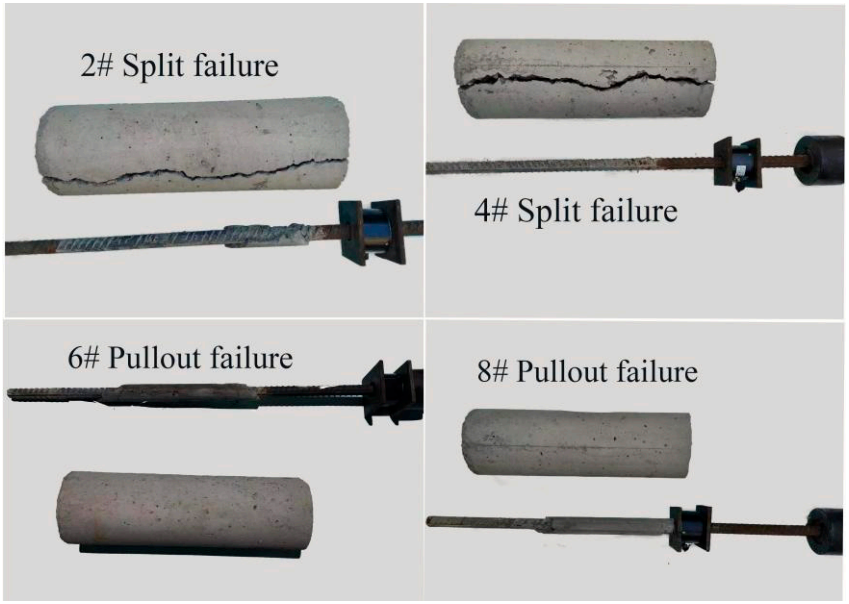


**Figure 6.** Damage pattern of specimen in grouted rockbolt systems.

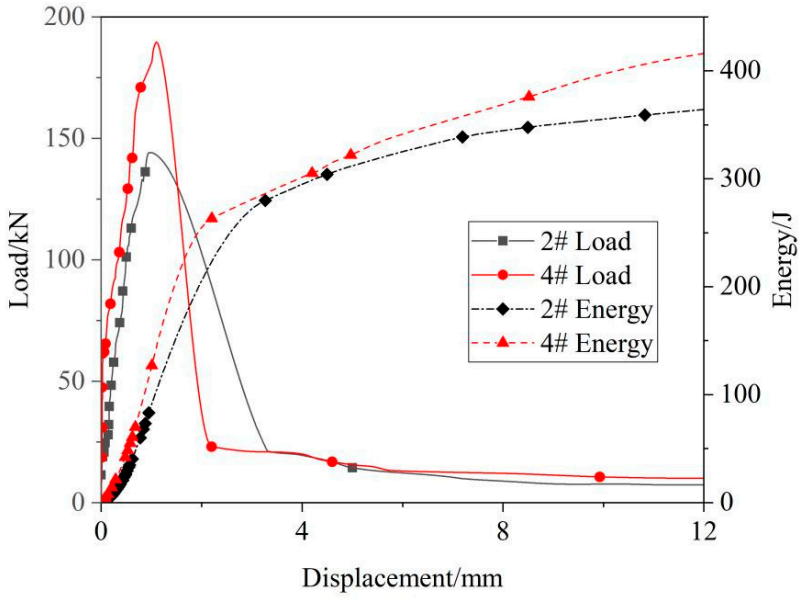


**Figure 7.** Relationship between pullout load, energy, and displacement in the grouted rockbolt system in the split failure mode.

Figure 8 shows the relationship between the peak load and the energy absorbed in the elastic phase of the specimen undergoing split failure. The energy absorbed in the elastic phase tends to increase with the increase in the peak load. When the load reaches its peak, the anchoring interface enters a soft stress state, the anchoring agent is crushed, and cracks develop inside the concrete. Most of the energy, as in more than 50%, absorbed by the rockbolt is consumed in this phase. The concrete produces through-body cracks with the pulling, and this causes anchorage interface debonding. At this time, the rate of energy absorption decreases sharply, and there is a clear inflection point; the energy absorbed by the rockbolt at this stage is mainly used to overcome the mechanical bite force of the anchorage interface, such that the absorbed energy is the lowest in the entire pulling process, 25.95 J, 53.24 J, 36.24 J, and 61.12 J, no more than the total energy of 15%.

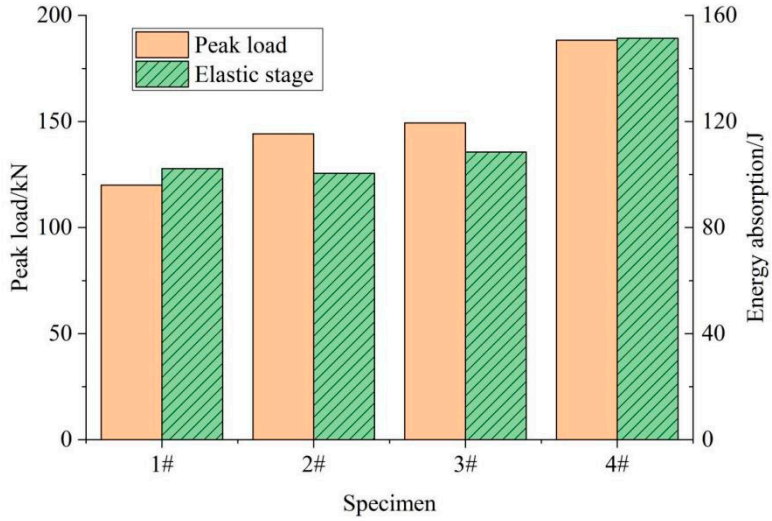


**Figure 8.** Peak load vs. energy absorption in elastic phase for grouted rockbolt systems in split failure mode.

Figure 9 shows the load vs. energy displacement relationship for specimens #6 and 8. The load decreases gradually with increasing slip after its peak, rather than decreasing sharply, as in the specimens that underwent the split failure mode. Different from the samples with split failure mode, there were no or only small cracks on the surface of the specimen, and the energy absorption rate gradually decreased without obvious inflection points. Before the load reached its peak value, the bonding stress development caused by the load acting on the rockbolt at the anchorage interface was similar to that under the split failure mode. When the load reached the peak value, the anchorage interface entered the softening stage, the free end of the anchoring agent showed a shear breaking phenomenon developing towards the loading end, and the anchorage interface gradually disappeared from the free end. Because the load reduction rate was lower than the crack development rate, the cracks formed along the parallel direction of the rockbolt were not enough to consume the energy absorbed by the rockbolt and form cracks perpendicular to the rockbolt. As a result, the anchoring agent broke, and the anchoring agent at the loading end pulled out with the rockbolt, so the energy absorbed by the rockbolt at this stage was higher than that of the split failure. When the anchorage interface was completely unglued, the energy absorbed by the rockbolt needed to overcome the mechanical bite force of the free end anchorage interface and the frictional resistance of the loading end, which resulted in the energy generated by the load acting on the rockbolt at the anchorage interface being higher than the split failure. At this stage, the energy absorbed by the rockbolt was 127.71 J, 130.02 J, 142.47 J and 150.1 J, accounting for more than 20% of the total energy absorbed. As can be seen from Figure 9, during the softening stage, the energy absorption rate of specimen #6 decreased significantly more than that of specimen #8. This is because cracks on the anchorage interface developed slowly under the pullout failure mode, and the load acting on the rockbolt of specimen #8 was higher than that of specimen #6, resulting in a significantly lower energy absorption rate of specimen #6 than that of specimen #8. In addition, since the bond stress was provided by the friction resistance and the mechanical bite force, the load reduction rate was low, so the energy absorption rate of the rockbolt changed little during the unglued stage.

Figure 10 shows the relationship between the peak load and the energy absorbed in the elastic phase of the specimen that underwent pullout failure. When the specimen underwent pullout failure, cracks developed slowly on the anchorage interface, and cracks may appear perpendicular to the rockbolt, which will lead to no obvious law in the change of absorbed energy at the elastic stage.

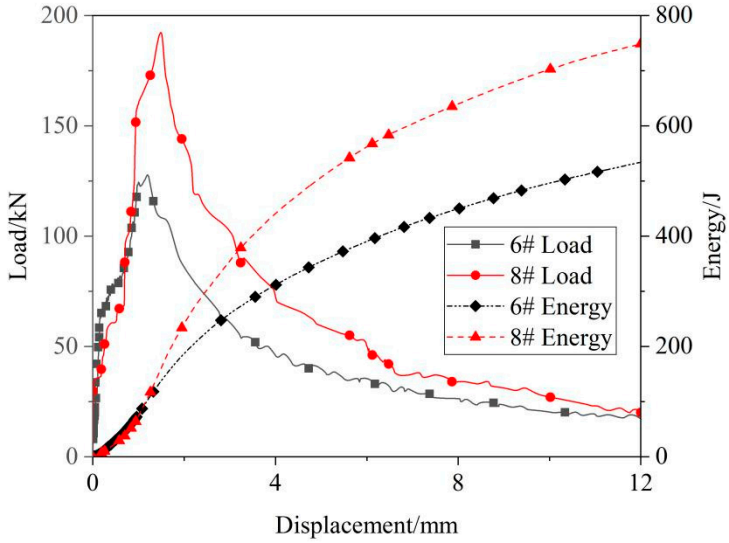


**Figure 9.** Relationship between pullout load, energy, and displacement in grouted rockbolt systems in pullout failure mode.

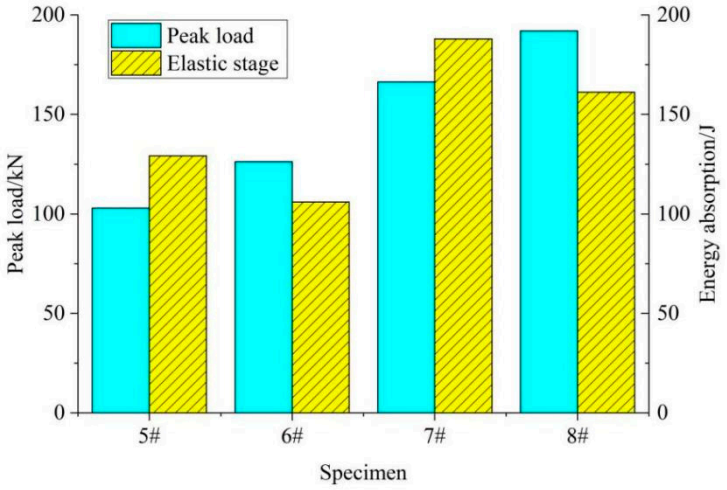


**Figure 10.** Peak load vs. energy absorption in the elastic phase for grouted rockbolt systems in pullout failure mode.

### *4.3. Analysis of Damage Mechanism of Grouted Rockbolt Systems*

Figure 11 shows a schematic diagram of the split failure occurring in the rockbolt bar anchoring structure. In the early stage of rockbolt pulling, with the increase in the pulling load rockbolt rib surface and anchoring agent detachment, the rockbolt was subjected to a micro-slip, causing an expansion in the cement mortar shear, and forcing the cement mortar to be radially displaced. The anchoring interface began to enter the shear expansion stress state from the elastic stress state. As the load continued to increase, the loaded end of the anchoring interface transformed from the shear expansion stress state into a soft stress state. As the load was transferred to the free end, the anchoring agent between the ribs of the anchor rod was constantly crushed and piled up in the anchor hole to produce a wedge plugging effect As the rockbolt slipped, the cracks developed rapidly and extended to the surface of the concrete, causing the interface softening region to develop further, resulting in splitting cracks, split failure in the anchor structure, the debonding of the interface between the rockbolt and the anchoring agent, and the pulling out of the rockbolt.

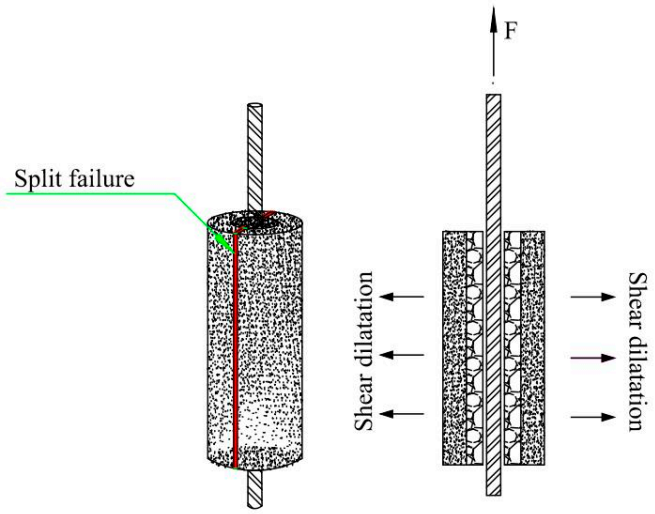


**Figure 11.** Schematic diagram of split failure.

Figure 12 shows the schematic diagram of a rockbolt anchoring structure undergoing pullout failure. The failure mechanism here is similar to that of split failure, except that two anchorage interface failure modes occurred with pullout failure: debonding occurred at the loaded end at the interface between the anchorage and the concrete, and at the free end at the interface between the rockbolt and the anchorage. Cracks first developed at the loading end, leading to debonding of the anchorage interface. The shear stress provided by the interface at the loading end decreased, such that the radial force generated inside the loading end was insufficient to allow the anchorage to break up under shear expansion stress. The interfacial shear stress reached its limit at the interface between the anchorage and the concrete, leading to debonding. As pullout proceeded, the debonding region developed from the loaded to the free end, the shear stress provided by the free end increased, and the anchorage at the free end was crushed under the shear expansion stress. The rockbolt and anchorage interface debonded until the rockbolt was pulled out, with a small amount of anchorage surviving at the loaded end. The anchorage was crushed at the free end, and there were no or small cracks on the surfaces of the grouted rockbolt systems.

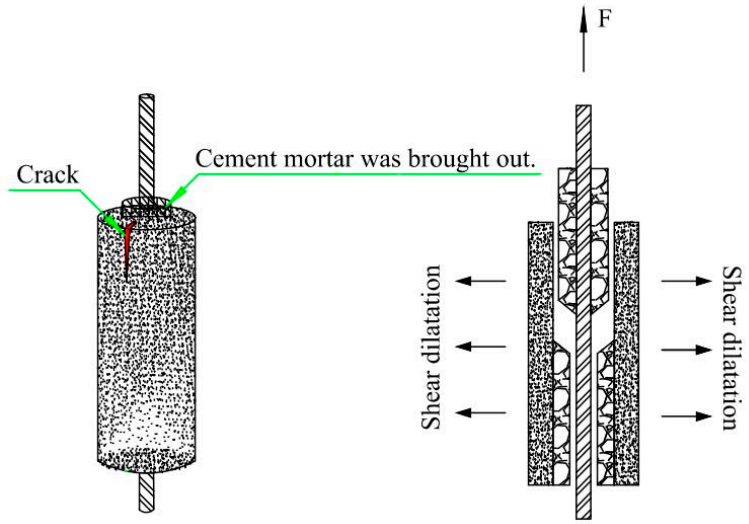


**Figure 12.** Schematic diagram of pullout failure.

## 5. Discussion

The failure modes of different specimens were obtained through indoor pullout tests; as shown in Figure 6, shear failure occurred at the anchorage interface under the pullout load. When split failure occurs, cracks parallel to the rockbolt will occur on the anchorage interface and develop along the direction that makes the rockbolt unglued, and the anchorage interface will be completely unglued. When pullout failure occurs, cracks perpendicular to the rockbolt will inevitably occur on the anchorage interface, leading to shear failure of the anchoring agent and the partial ungluing of the anchorage interface, which is also the reason why the energy consumption of pullout failure is higher than that of split failure. The development of cracks on the anchorage interface is similar to that shown in the experimental results of Foraboschi [30], which is similar to mode II of fracture mechanics. The difference is that the development direction of cracks on the anchorage interface under load results in different failure modes of the grouted rockbolt systems.

The failure process of the grouted rockbolt systems is the result of energy accumulation and release, but the different failure modes of the anchorage interface under load significantly affect the energy absorbed by the rockbolt. As can be seen from Table 2, the energy absorbed by split failure is lower than that absorbed by pullout failure, and the absorbed energy increases with the increase in peak load, which is similar to Yu's [23] test results. Yu considered cement mortars of different strengths as anchoring agents to conduct a pullout test on the specimen, and studied the energy absorbed by the rockbolt during the pullout process. However, this rule is limited to specimens under the same failure mode, and is not applicable under different failure modes. For example, the peak load of specimen #4 is 188.29 kN, the absorption energy is 420.40 J, and the peak load of specimen #5 is 103 kN, but the absorbed energy is 534.6 J; the peak load is low but the absorbed energy is large. Therefore, it is very important to study the energy dissipation under different failure modes.

## 6. Conclusions

This study investigates the relationship between the failure modes and energy dissipation of the grouted rockbolt systems under load by conducting indoor pullout tests. The results obtained can be summarized as follows:

1. The failure mode of the grouted rockbolt systems under pullout loading is closely related to the energy dissipation, and the absorbed energy of the rockbolt in pullout failure mode is higher than that in split failure mode. In the split failure mode, the energy absorption rate of the rockbolt decreases sharply at the end of the softening phase, which does not occur in the pullout failure mode;
2. Irrespective of whether the specimen undergoes split or pullout failure, in the softening stage, the grouted rockbolt systems absorb the most energy, accounting for more than 50% of the energy absorbed in the entire pulling process. In the split failure mode, the cracks on the anchorage interface develop along the direction that makes the rockbolt unglued, while in the pullout failure mode, the cracks on the anchorage interface not only produce cracks parallel to the rockbolt, but also produce cracks perpendicular to the rockbolt, which leads to the energy absorbed by pullout failure being higher than that during split failure;
3. The failure mode of specimen #1–4 is split failure. The bonding stress generated by the load acting on the rockbolt makes the anchorage interface unglued, and the bonding stress is greater than the shear strength of the anchorage interface. The anchorage interface is completely shear-destroyed and the rockbolt is pulled out, resulting in cracks in the whole body on the surrounding rock surface;
4. The failure mode of specimens #5–8 is pullout failure. In the pullout failure mode, due to cracks in the anchorage interface perpendicular to the rockbolt, the energy absorbed by the rockbolt is insufficient to cause shear failure at the anchorage interface at the loading end, resulting in shear failure at the free end of the anchorage interface, and the anchoring agent at the loading end is pulled out with the rockbolt.

**Author Contributions:** Methodology, S.Y.; Investigation, H.Y.; Data curation, Y.W.; Writing—review & editing, Y.W.; Supervision, S.L.; Funding acquisition, S.Y. All authors have read and agreed to the published version of the manuscript.

**Funding:** This work is funded by the National Science Foundation of China (Grant No. 52104157).

**Data Availability Statement:** All the data is included in the manuscript.

**Conflicts of Interest:** The authors declare no conflict of interest.

## References

1. Xie, H.P. Research progress of the mechanics and mining theory of deep rock mass. *J. China Coal. Soc.* **2019**, *44*, 2803–2813. (In Chinese)
2. Li, A.; Cui, G.; Wang, P.; Wang, X.; Hong, Z.; Kong, J.; Kan, J. Deformation and Failure Laws of Surrounding Rocks of Coal Roadways under High Dynamic Load and Intelligent Prediction. *Sustainability* **2023**, *15*, 1313. [CrossRef]
3. Wu, X.; Jiang, Y.; Gong, B.; Deng, T.; Guan, Z. Behaviour of rock joint reinforced by energy-absorbing rock bolt under cyclic shear loading condition. *Int. J. Rock. Mech. Min.* **2018**, *110*, 88–96. [CrossRef]
4. Wu, X.Y.; Jiang, L.S.; Xu, X.G.; Guo, T.; Zhang, P.P.; Huang, W.P. Numerical analysis of deformation and failure characteristics of deep roadway surrounding rock under static-dynamic coupling stress. *J. Cent. South. Univ.* **2021**, *28*, 542–555. [CrossRef]
5. Knox, G.; Hadjigeorgiou, J. Influence of Testing Configuration on the Performance of Paddled Energy-Absorbing Rockbolts Under Impact Loading. *Rock. Mech. Rock. Eng.* **2022**, *55*, 5705–5721. [CrossRef]
6. Kang, H.P. Research and practice of bolt support in deep rock burst roadway. *J. China Coal Soc.* **2015**, *40*, 2225–2233. (In Chinese)
7. Li, C.C.; Stjern, G.; Myrvang, A. A review on the performance of conventional and energy-absorbing rockbolts. *J. Rock. Mech. Geotech. Eng.* **2014**, *6*, 315–327. [CrossRef]
8. Wang, J.; Liu, W.; Song, Z.; Li, L.; Feng, S.; Cheng, Y. A new energy-absorbing bolt used for large deformation control of tunnel surrounding rock. *Int. J. Min. Sci. Techno.* **2022**, *32*, 1031–1043. [CrossRef]
9. Tahmasebinia, F.; Yang, A.; Feghali, P.; Skrzypkowski, K. A Numerical Investigation to Calculate Ultimate Limit State Capacity of Cable Bolts Subjected to Impact Loading. *Appl. Sci.* **2023**, *13*, 15. [CrossRef]
10. Zhao, T.B.; Guo, W.Y.; Yin, Y.C.; Tan, Y.L. Bolt pull-out tests of anchorage body under different loading rates. *Shock. Vib.* **2015**, *2015*, 121673. [CrossRef]
11. Li, E.; Feng, J.; Xie, H.; Zhang, H. Numerical Analysis of Anchor Bolt Pull-out Test by Cohesive Zone Model Combined with Finite Element Method. *IOP Conf. Ser. Earth Environ. Sci.* **2020**, *570*, 52014–52019. [CrossRef]
12. Ansell, A. Laboratory testing of a new type of energy absorbing rock bolt. *Tunn. Undergr. Space Tech.* **2005**, *20*, 291–300. [CrossRef]
13. Dai, L.; Pan, Y.; Wang, A.; Xiao, Y.; Ma, X. Experimental Study on the Self-Protection Performance of Anchor Bolts with Energy-Absorbing Tails. *Rock. Mech. Rock. Eng.* **2020**, *53*, 2249–2263. [CrossRef]
14. Wu, X.; Jiang, Y.; Guan, Z.; Wang, G. Estimating the support effect of energy-absorbing rock bolts based on the mechanical work transfer ability. *Int. J. Rock. Mech. Min.* **2018**, *103*, 168–178. [CrossRef]
15. Cai, M.; Champaigne, D.; Kaiser, P. Development of a fully debonded cone bolt for rockburst support. In Proceedings of the Fifth International Seminar on Deep and High Stress Mining, Santiago, Chile, 4–8 October 2010; pp. 329–342. [CrossRef]
16. Liang, Y.; He, M.; Cao, C.; Wang, S.; Ren, T. A mechanical model for conebolts. *Comput. Geotech.* **2017**, *83*, 142–151. [CrossRef]
17. Chen, Y.; Li, C.C. Performance of fully encapsulated rebar bolts and D-Bolts under combined pull-and-shear loading. *Tunn. Undergr. Space Tech.* **2015**, *45*, 99–106. [CrossRef]
18. Chen, J.; He, F.; Zhang, S. A study of the load transfer behavior of fully grouted rock bolts with analytical modelling. *Int. J. Min. Sci. Techno.* **2020**, *30*, 105–109. [CrossRef]
19. Foraboschi, P. Shear strength computation of reinforced concrete beams strengthened with composite materials. *Compos. Mech. Comput. A* **2012**, *3*, 227–252. [CrossRef]
20. Xu, X.; Tian, S. Load transfer mechanism and critical length of anchorage zone for anchor bolt. *PLoS ONE* **2020**, *15*, e0227539. [CrossRef] [PubMed]
21. Zhang, X.; Wu, Z.; Zheng, J.; Dong, W.; Bouchair, A. Ultimate bond strength of plain round bars embedded in concrete subjected to uniform lateral tension. *Constr. Build. Mater.* **2016**, *117*, 163–170. [CrossRef]
22. Li, X.; Wu, Z.; Zheng, J.; Liu, H.; Dong, W. Hysteretic Bond Stress-Slip Response of Deformed Bars in Concrete under Uniaxial Lateral Pressure. *J. Struct. Eng.* **2018**, *144*, 04018041. [CrossRef]
23. Yu, S.; Zhu, W.; Niu, L.; Zhou, S.; Kang, P. Experimental and numerical analysis of fully grouted long rockbolt load-transfer behavior. *Tunn. Undergr. Space Tech.* **2019**, *85*, 56–66. [CrossRef]
24. Sun, Z.; Zhang, D.; Fang, Q.; Liu, D.; Dui, G. Displacement process analysis of deep tunnels with grouted rockbolts considering bolt installation time and bolt length. *Comput. Geotech.* **2021**, *140*, 104437. [CrossRef]
25. Luga, E.; Periku, E. A pioneer in-situ investigation on the bearing capacity and failure causes of real scale fully grouted rockbolts. *Constr. Build. Mater.* **2021**, *310*, 124826. [CrossRef]
26. Epackachi, S.; Esmaili, O.; Mirghaderi, S.R.; Behbahani, A.A.T. Behavior of adhesive bonded anchors under tension and shear loads. *J. Constr. Steel Res.* **2015**, *114*, 269–280. [CrossRef]

27. Wang, B.; Bai, G.L. Research on the energy mechanism of the bonding and failure process of steel bar and reclaimed concrete. *Concrete* **2011**, *2*, 32–35. (In Chinese)
28. Xie, H.P.; Ju, Y.; Li, L.Y. Rock strength and overall destruction criterion based on the principle of energy dissipation and release. *J. Rock. Mech. Eng.* **2005**, *17*, 3003–3010.
29. Chen, X.G.; Zhang, Q.Y. Study on the energy dissipation and release of the rock shear failure process. *J. Min. Saf. Eng.* **2010**, *27*, 179–184.
30. Foraboschi, P. Predictive multiscale model of delayed debonding for concrete members with adhesively bonded external reinforcement. *Compos. Mech. Comput. A* **2012**, *3*, 307–329. [CrossRef]